International Journal of Solids and Structures 49 (2012) 1753–1763

Contents lists available at SciVerse ScienceDirect

International Journal of Solids and Structures

journal homepage: www.elsevier.com/locate/ijsolstr

An FE-MPEC approach for limit load evaluation in the presence of contact and displacement constraints

S. Tangaramvong [a,*], F. Tin-Loi [b]

[a] School of Civil, Environmental and Chemical Engineering, RMIT University, GPO Box 2476, Melbourne, VIC 3001, Australia
[b] School of Civil and Environmental Engineering, The University of New South Wales, Sydney, NSW 2052, Australia

ARTICLE INFO

Article history:
Received 15 November 2011
Received in revised form 15 February 2012
Available online 3 April 2012

Keywords:
Cohesive fracture
Complementarity problem
Frictional contact
Limit analysis
Mathematical programing
Mixed finite element

ABSTRACT

This paper describes a mathematical programing based approach for the direct limit load evaluation of a structural system under simultaneous contact and limited displacement conditions. The contact model we adopt can simulate either a classical unilateral (nonassociative) Coulomb friction situation or a cohesive fracture idealization at the potential discontinuity interface between contacting bodies. The discrete FE model is constructed using locking free mixed finite elements. The main feature and novelty of our proposed approach is to compute in a single step the maximum load capacity of the structure, such that both the imposed displacement limitations and the contact conditions are satisfied. In essence, the formulation is a nontrivial extension of classical limit analysis. The analysis is cast in its most natural form, namely in mixed static-kinematic variables, and leads to, what is known in the mathematical programing literature, as a mathematical program with equilibrium constraints or MPEC. A nonlinear programing (NLP) based algorithm is proposed to solve the MPEC. Two examples are provided to illustrate application of the proposed scheme, and some comments regarding the various advantages of the adopted mathematical programing framework are made.

1. Introduction

The safety assessment of structures for which discontinuities can arise has been the active subject of research interest over the last decades. Damage to these structures typically occurs in a narrow region between two or more bodies in contact, and forms an important consideration in various engineering applications. Moreover, this class of structures can be challenging to analyze. Some examples are: the failure of a concrete gravity dam promoted by hydraulic pressure (e.g. Alfano et al., 2006; Bolzon, 2010; Bolzon and Cocchetti, 2003); the frictional sliding contact of indented material and conical indenter (Bellemare et al., 2007); the microcracking damage of concrete-like, quasi-brittle materials (e.g. Maier et al., 1993; Tin-Loi and Que, 2001); the frictional contact problem of homogeneous bodies (e.g. Christensen, 2002; Dong, 1999; Kanno and Ohsaki, 2011; Tin-Loi and Xia, 2001); and the decohesion process of mortar joints in masonry structures (e.g. Ferris and Tin-Loi, 2001; Giambanco et al., 2001; Gilbert et al., 2006).

The analysis of structures that can form strong discontinuities is typically carried out in an evolutive (step-by-step) fashion. Without doubt, a rich and full spectrum of load and deformation responses can be obtained, enabling, for instance, the behavior of the structure at any prescribed load (or displacement) level to be monitored. These step-by-step procedures will of necessity perform numerical integration of the constitutive laws describing the inelastic, intrinsic path-dependent (nonholonomic) material behavior of the structure using some iterative type (e.g. predictor–corrector) algorithm often based on a consistent tangent concept (e.g. Simo and Hughes, 1998; Simo and Taylor, 1985). However, such a numerical method can involve extensive computational effort since the implementation of the current step is based on the knowledge of the previous step. Moreover, the presence of physically instabilizing phenomena, such as strain softening, invariably adds to the already large number of iterations for each, often very small, incremental step.

Motivated by the simplicity and, at the same time, usefulness of so-called direct and simplified analyses typified by classical limit (Kamenjarzh, 1996) and shakedown analyses, an increasingly appealing alternative is to compute directly the maximum load capacity the structure can sustain, even in the presence of such nontraditional inclusions as nonassociativity, softening and ductility constraints.

In recent times, there has been considerable research effort in the extension of key ideas underpinning the mathematical programing approach to classical discrete limit analyses, as pioneered by Maier and his colleagues (e.g. Maier, 1970, 1984; Maier and Munro, 1982), to include such afore-mentioned constraints (e.g. Ardito et al., 2008; Bolzon, 2010; Bolzon and

* Corresponding author. Tel.: +61 3 9925 0806; fax: +61 3 9639 0138.
E-mail address: s.tangaramvong@rmit.edu.au (S. Tangaramvong).

0020-7683/$ - see front matter © 2012 Elsevier Ltd. All rights reserved.
http://dx.doi.org/10.1016/j.ijsolstr.2012.03.022

Cocchetti, 2003; Ferris and Tin-Loi, 2001; Tangaramvong and Tin-Loi, 2011a). In all cases, the formulation no longer takes the form of a classical convex nonlinear programing (NLP) problem, but leads to an instance of the challenging class of mathematical programing problems known as a mathematical program with equilibrium constraints or MPEC (Luo et al., 1996)—a problem type anticipated some 30 years ago by Maier, who referred to these as optimization under complementarity constraints (Maier, 1984; Maier and Munro, 1982). In our context, the complementarity constraints are precisely the equilibrium constraints, and embody the necessary conditions that govern the inelastic constitutive behavior of the structural system. Theoretically, such MPECs, in view of their nonconvexity and nonsmoothness, can pose both numerical and theoretical difficulties. However, our computational experience is more positive, as it appears that for practical engineering problems various NLP-based schemes can reliably and efficiently process the MPEC (e.g. Ferris and Tin-Loi, 2001; Tangaramvong and Tin-Loi, 2011a).

The present paper provides a further contribution to the MPEC approach for computing the limit-state capacity of structures. In particular, we carry out a maximum load evaluation, within a small deformation regime, of a structure subjected to conditions pertaining, simultaneously, to contact and limited displacements. Elastoplastic material behavior can be robustly accommodated within the mixed FE framework developed.

The main features of the proposed approach are as follows. First, through the use of a high level mathematical programing framework (GAMS—an acronym for General Algebraic Modeling System) the handling of the nonlinear complementarity conditions (Brooke et al., 1998), that arise due to material inelasticity and contact relations, does not require the use of any onerous outer level iterative procedures. Second, the MPEC can be solved efficiently and reliably by an iterative adaptation of a standard NLP solution scheme. Third, the use of the bilinear mixed (plane stress or plane strain) finite element (FE) developed by Capsoni and Corradi (1997a,b) provides coarse mesh accuracy and avoids the well-known incompressibility locking. Finally, the contact relations at the loci of potential discontinuities can be written to either describe unilateral and nonassociative Coulomb friction or a cohesive fracture law, as illustrated by variants of two well-known problems, namely regarding two elastoplastic bodies in contact (Dong, 1999) and a concrete gravity dam subjected simultaneously to a nonlinear exponential traction decay and a hydraulic uplift pressure (ICOLD, 1999).

As for organization of this paper, the next Section 2 presents all the basic ingredients, namely statics, kinematics, constitutive laws and contact conditions, governing the discrete FE model. The model appropriately assumes a path-independent (holonomic) behavior since, within the context of proportionally applied load regimes, holonomy provides a sufficiently accurate prediction of the actual path-dependent behaviors (Tangaramvong and Tin-Loi, 2007). As a preliminary to the MPEC approach, these relations are collected and manipulated in their most natural form to furnish a mixed complementarity problem or MCP (Dirkse and Ferris, 1995; Rutherford, 1995). The proposed direct maximum load approach is then formulated as an MPEC. Several NLP-based algorithms capable of solving the MPEC are then briefly described in Section 3. In Section 4, two contact examples, one related to a well-known frictional contact problem (Dong, 1999) and the other to a benchmark concrete gravity dam (ICOLD, 1999), are provided to illustrate application of our scheme. The accuracy of the MPEC results is also validated using the associated stepwise holonomic responses. Finally, some pertinent concluding remarks are drawn in Section 5.

A word regarding notation is in order. Vectors and matrices are indicated in bold. A real vector $\mathbf{x}$ of size m is indicated by $\mathbf{x} \in \Re^m$ and a real $m \times n$ matrix $\mathbf{A}$ by $\mathbf{A} \in \Re^{m\times n}$. For brevity, a vector of functions $\mathbf{f}(\mathbf{x}) : \Re^m \to \Re^n$ is written simply as $\mathbf{f} \in \Re^n$.

2. Generic FE model

We consider a suitably discretized FE model of an elastoplastic structure for which contact-like conditions can be enforced at some a priori defined interface pairs. Such conditions can describe not only Coulomb (and other) unilateral friction (Tangaramvong and Tin-Loi, 2011a; Tin-Loi and Xia, 2001), but also a discrete cohesive crack behavior (Bolzon and Cocchetti, 2003; Tin-Loi and Que, 2001).

The FE model we adopt is expressed in intrinsic, natural variables, in Prager's generalized sense (Maier, 1970). More explicitly, the scalar product of generalized stress $\mathbf{Q}^{\mathbf{i}}$ and strain $\mathbf{p}^{\mathbf{i}}$ vectors represents virtual work of the element i. It is notable that rigid body motions are precluded from such an element and the material behavior is directly reflected by the elemental behavior.

The loads are proportionally prescribed through a single load multiplier α and are applied as nodal forces; distributed loads are simulated as a suitable number of equivalent concentrated forces. Thus, within the global reference axis system, the unconstrained nodal forces at a generic node i can be expressed as $\alpha\mathbf{f}^{\mathbf{i}} + \mathbf{f}^{\mathbf{i}}_d$, namely in terms of the load multiplier α, the given basic nodal forces $\mathbf{f}^{\mathbf{i}}$ and the fixed nodal forces $\mathbf{f}^{\mathbf{i}}_d$.

The constitutive model expressing intrinsic material and contact behaviors is assumed, in the spirit of deformation theory of plasticity, to follow a holonomic (path-independent) law. This simplifying assumption entails reversibility of plastic strains and interface translations, for which the existence of any local unloading is prohibited. The governing relations can thus be conveniently written in total quantities, rather than rate terms as for a nonholonomic (path-dependent) model. The holonomy hypothesis is reasonable since, within the assumed monotonically applied loading regime, extensive unloading is unlikely to occur. Even if unloadings do occur, the global responses of the structure based on holonomic conditions are largely insensitive to such events, and are essentially identical to those based on the exact nonholonomic assumption (Tangaramvong and Tin-Loi, 2007).

2.1. Governing relations

In terms of well-known FE notation and description (e.g. Maier, 1970; Tangaramvong and Tin-Loi, 2011a), the governing holonomic relations of the whole structural system (that has been suitably discretized into n elements, d degrees of freedom, m natural generalized stresses or strains, y plastic yield functions, c potential contact points, and x contact conditions) can be written compactly as follows:

$$\mathbf{C}^{\mathrm{T}}\mathbf{Q} = \alpha\mathbf{f} + \mathbf{f}_d - \mathbf{C}_n^{\mathrm{T}}\mathbf{r}_n - \mathbf{C}_t^{\mathrm{T}}\mathbf{r}_t, \tag{1}$$

$$\mathbf{q} = \mathbf{C}\mathbf{u}, \tag{2}$$

$$\mathbf{Q} = \mathbf{E}(\mathbf{q} - \mathbf{p}), \tag{3}$$

$$\mathbf{p} = \frac{\partial \mathbf{w}^{\mathrm{T}}}{\partial \mathbf{Q}}\boldsymbol{\lambda}, \tag{4}$$

$$-\mathbf{w}(\mathbf{Q}, \mathbf{p}, \mathbf{r}) \geqslant \mathbf{0}, \quad \boldsymbol{\lambda} \geqslant \mathbf{0}, \quad \mathbf{w}^{\mathrm{T}}\boldsymbol{\lambda} = 0, \tag{5}$$

$$\mathbf{V}_t\boldsymbol{\zeta} = \mathbf{C}_t\mathbf{u}, \tag{6}$$

$$\boldsymbol{\pi}_n = \mathbf{V}_n\boldsymbol{\zeta} - \mathbf{C}_n\mathbf{u} \geqslant \mathbf{0}, \quad \mathbf{r}_n \geqslant \mathbf{0}, \quad \boldsymbol{\pi}_n^{\mathrm{T}}\mathbf{r}_n = 0, \tag{7}$$

$$\boldsymbol{\pi}_c = -\mathbf{N}_n^{\mathrm{T}}\mathbf{r}_n - \mathbf{N}_t^{\mathrm{T}}\mathbf{r}_t + \mathbf{r}_c \geqslant \mathbf{0}, \quad \boldsymbol{\zeta} \geqslant \mathbf{0}, \quad \boldsymbol{\pi}_c^{\mathrm{T}}\boldsymbol{\zeta} = 0. \tag{8}$$

In view of the assumption of a small deformation regime, both equilibrium and compatibility conditions are linear. Equilibrium between external forces $\alpha\mathbf{f} + \mathbf{f}_d \in \Re^d$, resultant interface forces $\mathbf{r}_n, \mathbf{r}_t \in \Re^c$ and member generalized stresses $\mathbf{Q} \in \Re^m$ is described

in (1). At a generic contact interface $k \in \Gamma_c$, as shown in Fig. 1, the resultant forces (namely a normal force r_n^k acting along a normal direction and a tangential force r_t^k in a tangential direction) are transmitted between a pair of contact points associated with the two bodies I and II, where r_n^k is positive in compression. $\Gamma_c = \{1, \ldots, c\}$ collects a set of a priori known discrete contact interfaces (or joints). Compatibility between the generalized strains $\mathbf{q} \in \Re^m$ and the nodal displacements $\mathbf{u} \in \Re^d$ is expressed in (2) through a constant compatibility matrix $\mathbf{C} \in \Re^{m \times d}$.

The constitutive relations (3)–(5) describe a holonomic elasto-plastic material behavior. In particular, (3) reflects linear elasticity through an elastic (symmetric and positive definite) stiffness matrix $\mathbf{E} \in \Re^{m \times m}$. The associative flow rule in (4) expresses generalized plastic strains $\mathbf{p} \in \Re^m$ as functions of plastic multipliers $\boldsymbol{\lambda} \in \Re^y$ using the normality condition, thus ensuring that $\mathbf{p}$ is normal to the yield surface. The holonomic behavior is described by complementarity conditions in (5) involving two sign-constrained variables, namely yield functions $\mathbf{w} \in \Re^y \leqslant \mathbf{0}$ and plastic multipliers $\boldsymbol{\lambda} \geqslant \mathbf{0}$. Functions $\mathbf{w}(\mathbf{Q}, \mathbf{p}, \mathbf{r})$ are assumed to be homogeneous of order one, and thus can be expressed as functions of the generalized stresses $\mathbf{Q}$, the generalized plastic strains $\mathbf{p}$ and the current yield limits $\mathbf{r}$. The complementarity conditions ($\mathbf{w}^T\boldsymbol{\lambda} = 0$), it is worth mentioning, establish a componentwise relationship $w_j \leqslant 0$, $\lambda_j \geqslant 0$ and $w_j\lambda_j = 0$ for all j. Mechanically, they allow reversibility of plastic strains, and ensure that plastic activation occurs only when the stress point is on the yield surface.

For a unilateral frictional contact problem, the conditions at any one of the contact interfaces Γ_c are described by the three relations (6)–(8). Compatibility between the relative tangential displacements $\mathbf{C}_t\mathbf{u}$ at the contact interfaces and the associated tangential translations $\mathbf{V}_t\boldsymbol{\zeta}$ is specified in (6), where $\mathbf{C}_t \in \Re^{c \times d}$, $\mathbf{V}_t \in \Re^{c \times x}$ and $\boldsymbol{\zeta} \in \Re^x$. The Signorini conditions enforcing nonpenetration at the interfaces are represented by complementarity relations in (7), where $\mathbf{V}_n \in \Re^{c \times x}$, $\mathbf{C}_n \in \Re^{c \times d}$ and $\boldsymbol{\pi}_n \in \Re^c$. Clearly, the interface tractions ($\mathbf{r}_n \geqslant \mathbf{0}$) in the normal direction are sign-constrained, thus ensuring compression only for nonzero values. Finally, the contact constitutive law is represented by a further complementarity relation in (8) and describes the conditions defining activation and deactivation of the contact interfaces, where $\mathbf{N}_n$, $\mathbf{N}_t \in \Re^{c \times x}$ and $\mathbf{r}_c, \boldsymbol{\pi}_c \in \Re^x$. It is worth noting that the described contact law becomes associative if the pair of transformation matrices $\mathbf{N}_n$ and $\mathbf{V}_n$ ($\mathbf{N}_t$ and $\mathbf{V}_t$) are identical, i.e. $\mathbf{N}_n = \mathbf{V}_n$ and $\mathbf{N}_t = \mathbf{V}_t$.

For a cohesive crack problem, the two sets of relations (6) and (8) are retained, and (7) must be replaced by

$$\mathbf{V}_n\boldsymbol{\zeta} = \mathbf{C}_n\mathbf{u}. \tag{9}$$

The compatibility relations in (9) permit tensile tractions in the normal direction, as is necessary during a cohesive crack propagation.

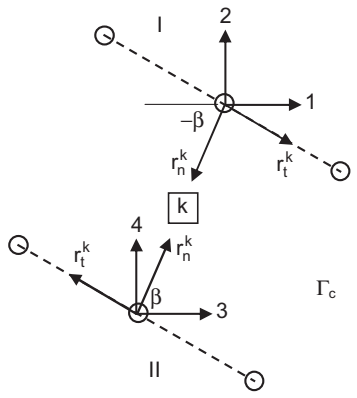

Fig. 1. Generic contact interface k.

2.2. Holonomic state problem

The holonomic state problem is formulated by simply collecting the four basic ingredients, namely statics (1), kinematics (2), material laws (3)–(5) and contact relationships (6)–(8) for the frictional contact problem or (6), (8), (9) for the cohesive fracture problem. In terms of mixed static-kinematic variables $(\mathbf{Q}, \mathbf{u}, \boldsymbol{\lambda}, \mathbf{r}_n, \mathbf{r}_t, \boldsymbol{\zeta})$, the state problems can then be written as follows.

For the frictional contact problem:

$$\begin{aligned}
&\mathbf{C}^T\mathbf{Q} + \mathbf{C}_\mathbf{n}^T\mathbf{r}_\mathbf{n} + \mathbf{C}_\mathbf{t}^T\mathbf{r}_\mathbf{t} - \alpha\mathbf{f} - \mathbf{f}_\mathbf{d} = \mathbf{0},\\
&\mathbf{Q} - \mathbf{E}\left(\mathbf{C}\mathbf{u} - \frac{\partial \mathbf{w}^T}{\partial \mathbf{Q}}\boldsymbol{\lambda}\right) = \mathbf{0},\\
&-\mathbf{w}(\mathbf{Q}, \mathbf{p}, \mathbf{r}) \geqslant \mathbf{0}, \quad \boldsymbol{\lambda} \geqslant \mathbf{0}, \quad \mathbf{w}^T\boldsymbol{\lambda} = 0,\\
&-\mathbf{C}_\mathbf{t}\mathbf{u} + \mathbf{V}_\mathbf{t}\boldsymbol{\zeta} = \mathbf{0},\\
&\boldsymbol{\pi}_n = \mathbf{V}_\mathbf{n}\boldsymbol{\zeta} - \mathbf{C}_\mathbf{n}\mathbf{u} \geqslant \mathbf{0}, \quad \mathbf{r}_\mathbf{n} \geqslant \mathbf{0}, \quad \boldsymbol{\pi}_n^T\mathbf{r}_\mathbf{n} = 0,\\
&\boldsymbol{\pi}_c = -\mathbf{N}_n^T\mathbf{r}_n - \mathbf{N}_t^T\mathbf{r}_t + \mathbf{r}_c \geqslant \mathbf{0}, \quad \boldsymbol{\zeta} \geqslant \mathbf{0}, \quad \boldsymbol{\pi}_c^T\boldsymbol{\zeta} = 0.
\end{aligned} \tag{10}$$

For the cohesive fracture problem:

$$\begin{aligned}
&\mathbf{C}^T\mathbf{Q} + \mathbf{C}_n^T\mathbf{r}_n + \mathbf{C}_t^T\mathbf{r}_t - \alpha\mathbf{f} - \mathbf{f}_d = \mathbf{0},\\
&\mathbf{Q} - \mathbf{E}\left(\mathbf{C}\mathbf{u} - \frac{\partial \mathbf{w}^T}{\partial \mathbf{Q}}\boldsymbol{\lambda}\right) = \mathbf{0},\\
&-\mathbf{w}(\mathbf{Q}, \mathbf{p}, \mathbf{r}) \geqslant \mathbf{0}, \quad \boldsymbol{\lambda} \geqslant \mathbf{0}, \quad \mathbf{w}^T\boldsymbol{\lambda} = 0,\\
&-\mathbf{C}_t\mathbf{u} + \mathbf{V}_t\boldsymbol{\zeta} = \mathbf{0},\\
&-\mathbf{C}_n\mathbf{u} + \mathbf{V}_n\boldsymbol{\zeta} = \mathbf{0},\\
&\boldsymbol{\pi}_c = -\mathbf{N}_n^T\mathbf{r}_n - \mathbf{N}_t^T\mathbf{r}_t + \mathbf{r}_c \geqslant \mathbf{0}, \quad \boldsymbol{\zeta} \geqslant \mathbf{0}, \quad \boldsymbol{\pi}_c^T\boldsymbol{\zeta} = 0.
\end{aligned} \tag{11}$$

Both of these systems (10) or (11) are square and involve complementarity relations. They can be recognized as being special instances of a class of important mathematical programing problems, namely MCPs (e.g. Dirkse and Ferris, 1995; Rutherford, 1995). These problems are similar to the more well-known linear complementarity problem or LCP (Cottle et al., 1992), except that the MCP additionally contains free variables and can accommodate nonlinear relations, such as the nonlinear yield ($\mathbf{w}$) and contact ($\boldsymbol{\pi}_c$) functions, in our case.

For a holonomic analysis under load control, the response of the structure associated with a prescribed load multiplier α can be obtained by solving either MCP (10) for the frictional contact problem or MCP (11) for the cohesive crack problem. To obtain a full spectrum of holonomic structural responses, a series of MCP solves corresponding to various prescribed load levels α will need to be carried out. Usually, the presence of nonlinear constitutive relations requires the use of some iterative type numerical technique (e.g. Simo and Hughes, 1998; Simo and Taylor, 1985). In our case, we avoid this by processing the problem directly as an MCP by using the industry-standard solver GAMS/PATH (Dirkse and Ferris, 1995) available from within the powerful GAMS mathematical programing framework (Brooke et al., 1998).

2.3. Direct maximum load evaluation as an MPEC

The current subsection outlines the main idea underpinning our proposed direct maximum or limit load evaluation approach. It not only preserves the advantageous single-step feature of the classical limit analysis approach, but it can also cater for additional constraints that are associated with contact, fracture and serviceability limits.

Our starting point is the appropriate MCP (10) or (11), for which α is prescribed. If we now treat the driving parameter α as a variable, we can easily set up an optimization problem to attempt its maximization. The constraints of this maximization problem are explicitly given by (10) or (11). Any additional constraints, such

as displacement limits at specific points, can be simply added to the problem.

The formulations for direct maximum load method can then be written as the following (nonstandard) optimization problems in variables $(\alpha, \mathbf{Q}, \mathbf{u}, \boldsymbol{\lambda}, \mathbf{r}_n, \mathbf{r}_t, \boldsymbol{\zeta})$.

For the frictional contact problem:

$$\begin{array}{ll} \text{maximize} & \alpha \\ \text{subject to} & \text{MCP (10)} \\ & \text{displacement and other constraints.} \end{array} \tag{12}$$

For the cohesive fracture problem:

$$\begin{array}{ll} \text{maximize} & \alpha \\ \text{subject to} & \text{MCP (11)} \\ & \text{displacement and other constraints.} \end{array} \tag{13}$$

Problems (12) and (13) are nonstandard in view of the complementarity (or so-called equilibrium constraints in mathematical programing). They both belong to the challenging class of optimization programs, known in the literature as an MPEC (Luo et al., 1996).

MPECs originated in the form of "bilevel" programs in the 1970s, and has since become an active area of study both for its theoretical value and practical application in engineering and economics (Ferris and Pang, 1997). The presence of the complementarity constraints makes an MPEC disjunctive, and its solution is therefore often associated with severe computing costs, as would be expected of any combinatorial problem. In addition, the feasible region of the MPEC is not necessarily convex and may not even be connected. The monograph of Luo et al. (1996) provides an in-depth theoretical treatment (and some optimality conditions) of MPECs. However, the development of algorithms, guaranteed to converge and capable of processing successfully practical and large-size MPECs likely to arise in realistic applications, has yet to be achieved.

In spite of these difficulties, we have had considerable success in solving MPECs that arise in various engineering mechanics applications (e.g. Tangaramvong and Tin-Loi, 2011a,b; Tin-Loi and Que, 2001). Although we cannot guarantee convergence (let alone a global optimum), we have been able to obtain practically significant and in most cases verifiable solutions. The particular approach we have used involves reformulating the MPEC as a standard NLP problem by suitably transforming the complementarity conditions. Some of these iterative NLP-based schemes are described in the following section.

3. MPEC solution approaches

The generic solution approach we adopt to solve an MPEC, such as the one given in (12) or (13), exploits the use of some parametric reformulation that transforms the MPEC into a standard NLP problem. In essence, the nonconvex complementarity constraints are parameterized by a positive scalar μ, such that the original complementarity conditions become increasingly satisfied as μ is increased (or decreased, depending on the particular implementation). The reformulated MPEC therefore needs to be solved as a series of NLP subproblems with the aim of satisfying complementarity.

Such schemes are attractive since each subproblem is a standard NLP problem, and any general purpose NLP solver can be used. In our study, we used the GAMS/CONOPT solver (Drud, 1994).

Several such MPEC reformulations have been developed. The three we have implemented are named after the way complementarity is treated. They are: penalization, smoothing and relaxation. For simplicity of exposition, let us write the complementarity condition as $a \geqslant 0,\ b \geqslant 0$ and $ab = 0$.

(a) Penalization transfers all complementarity terms to the objective function, and penalizes them as $-\mu ab$. The penalty parameter μ is increased at each NLP iterate (e.g. Bolzon and Cocchetti, 2003; Tangaramvong and Tin-Loi, 2011b) until the required tolerance on the complementarity term has been reached.

(b) Smoothing replaces a complementarity condition using some smoothing equation. The particular one we prefer is the well-known Fischer-Burmeister function (Kanzow, 1996): $\psi_\mu(a,b) = \sqrt{a^2 + b^2 + 2\mu} - (a+b)$. The function ψ_μ has the property that $\psi_\mu(a,b) = 0$ if and only if $a \geqslant 0$, $b \geqslant 0$ and $ab = \mu$. The parameterization ψ_μ is a smoothing of the mapping $\psi_{\mu=0}$ implying that it is differentiable for nonzero μ. Again a series of NLP subproblems are solved while iteratively reducing the smoothing parameter μ (e.g. Tangaramvong and Tin-Loi, 2011a; Tin-Loi and Que, 2001).

(c) Relaxation replaces complementarity by its relaxed version $(ab \leqslant \mu)$. Smaller values of μ are successively applied to the NLP subproblems (e.g. Ferris and Tin-Loi, 2001; Tangaramvong et al., 2011).

The best method appears to be problem dependent. Moreover, from the large number of numerical examples we have tested, all these three NLP-based approaches had no difficulty in solving the MPECs given in (12) and (13). The penalty approach performed better in terms of efficiency and robustness, and is thus our preferred scheme.

The penalty subproblems for our MPECs can be written as follows.

For the friction contact problem:

$$\begin{aligned} \text{maximize}\ & \alpha - \boldsymbol{\mu}\left(-\mathbf{w}^{\mathrm{T}}\boldsymbol{\lambda} + \boldsymbol{\pi}_c^{\mathrm{T}}\boldsymbol{\zeta} + \boldsymbol{\pi}_n^{\mathrm{T}}\mathbf{r}_n\right) \\ \text{subject to}\ & \mathbf{C}^{\mathrm{T}}\mathbf{Q} + \mathbf{C}_n^{\mathrm{T}}\mathbf{r}_n + \mathbf{C}_t^{\mathrm{T}}\mathbf{r}_t - \alpha\mathbf{f} - \mathbf{f}_d = \mathbf{0}, \\ & \mathbf{Q} - \mathbf{E}\left(\mathbf{C}\mathbf{u} - \frac{\partial \mathbf{w}^{\mathrm{T}}}{\partial \mathbf{Q}}\boldsymbol{\lambda}\right) = \mathbf{0}, \\ & -\mathbf{w}(\mathbf{Q},\mathbf{p},\mathbf{r}) \geqslant \mathbf{0}, \quad \boldsymbol{\lambda} \geqslant \mathbf{0}, \\ & -\mathbf{C}_t\mathbf{u} + \mathbf{V}_t\boldsymbol{\zeta} = \mathbf{0}, \\ & \boldsymbol{\pi}_n = \mathbf{V}_n\boldsymbol{\zeta} - \mathbf{C}_n\mathbf{u} \geqslant \mathbf{0}, \quad \mathbf{r}_n \geqslant \mathbf{0}, \\ & \boldsymbol{\pi}_c = -\mathbf{N}_n^{\mathrm{T}}\mathbf{r}_n - \mathbf{N}_t^{\mathrm{T}}\mathbf{r}_t + \mathbf{r}_c \geqslant \mathbf{0}, \quad \boldsymbol{\zeta} \geqslant \mathbf{0}, \\ & \text{displacement and other constraints.} \end{aligned} \tag{14}$$

For the cohesive fracture problem:

$$\begin{aligned} \text{maximize}\ & \alpha - \boldsymbol{\mu}\left(-\mathbf{w}^{\mathrm{T}}\boldsymbol{\lambda} + \boldsymbol{\pi}_c^{\mathrm{T}}\boldsymbol{\zeta}\right) \\ \text{subject to}\ & \mathbf{C}^{\mathrm{T}}\mathbf{Q} + \mathbf{C}_n^{\mathrm{T}}\mathbf{r}_n + \mathbf{C}_t^{\mathrm{T}}\mathbf{r}_t - \alpha\mathbf{f} - \mathbf{f}_d = \mathbf{0}, \\ & \mathbf{Q} - \mathbf{E}\left(\mathbf{C}\mathbf{u} - \frac{\partial \mathbf{w}^{\mathrm{T}}}{\partial \mathbf{Q}}\boldsymbol{\lambda}\right) = \mathbf{0}, \\ & -\mathbf{w}(\mathbf{Q},\mathbf{p},\mathbf{r}) \geqslant \mathbf{0}, \quad \boldsymbol{\lambda} \geqslant \mathbf{0}, \\ & -\mathbf{C}_t\mathbf{u} + \mathbf{V}_t\boldsymbol{\zeta} = \mathbf{0}, \\ & -\mathbf{C}_n\mathbf{u} + \mathbf{V}_n\boldsymbol{\zeta} = \mathbf{0}, \\ & \boldsymbol{\pi}_c = -\mathbf{N}_n^{\mathrm{T}}\mathbf{r}_n - \mathbf{N}_t^{\mathrm{T}}\mathbf{r}_t + \mathbf{r}_c \geqslant \mathbf{0}, \quad \boldsymbol{\zeta} \geqslant \mathbf{0}, \\ & \text{displacement and other constraints.} \end{aligned} \tag{15}$$

A negative penalty, either $-\boldsymbol{\mu}\left(-\mathbf{w}^{\mathrm{T}}\boldsymbol{\lambda} + \boldsymbol{\pi}_c^{\mathrm{T}}\boldsymbol{\zeta} + \boldsymbol{\pi}_n^{\mathrm{T}}\mathbf{r}_n\right)$ or $-\boldsymbol{\mu}\left(-\mathbf{w}^{\mathrm{T}}\boldsymbol{\lambda} + \boldsymbol{\pi}_c^{\mathrm{T}}\boldsymbol{\zeta}\right)$ is used because of the maximization requirement.

The penalty algorithm attempts to iteratively solve NLP (14) or (15) for successively higher values of μ until a preset tolerance on the complementarity (e.g. $-\mathbf{w}^{\mathrm{T}}\boldsymbol{\lambda} + \boldsymbol{\pi}_c^{\mathrm{T}}\boldsymbol{\zeta} + \boldsymbol{\pi}_n^{\mathrm{T}}\mathbf{r}_n \leqslant 10^{-6}$ or $-\mathbf{w}^{\mathrm{T}}\boldsymbol{\lambda} + \boldsymbol{\pi}_c^{\mathrm{T}}\boldsymbol{\zeta} \leqslant 10^{-6}$) has been achieved.

4. Illustrative examples

Two examples, often used as benchmark structures (albeit with differing properties), are provided in this section to illustrate application of the proposed direct limit load approach.

The first example (Dong, 1999) concerns two blocks in unilateral frictional contact. In addition to purely elastic blocks as used in the source example, we also considered the case of two plane strain blocks made of a von Mises elastoplastic material. The second example considers the failure analysis of the well-known concrete gravity dam referenced by the International Committee on Large Dams (ICOLD, 1999). This example has often been used as a benchmark to test various numerical algorithms (e.g. Alfano et al., 2006; Bolzon, 2010; Bolzon and Cocchetti, 2003). In our study, Mode I quasibrittle fracture was assumed along a priori known potential damaging interfaces. Two cases, namely one realistically accounting for hydraulic uplift pressure and the other assuming a perfect drainage (thus eliminating uplift pressure) were analyzed.

For both examples, the accuracy of the direct limit load evaluation was validated through a comparison with the associated stepwise holonomic structural responses. Such stepwise holonomic analyses, it is worth mentioning, provide not only a sufficiently accurate prediction of the actual path-dependent structural behavior (Tangaramvong and Tin-Loi, 2011b), but can also be carried out very efficiently through an active set strategy (e.g. Ardito et al., 2008; Tangaramvong and Tin-Loi, 2011b) that considers only the yield functions likely to be active during the specified incremental step.

Both the direct limit load approach and the stepwise holonomic analysis were implemented as MATLAB codes, linked to the GAMS mathematical programing environment through a MATLAB-GAMS interface (Ferris, 1998). The solvers adopted were CONOPT and PATH for the NLP and MCP runs, respectively. For all MPEC runs, the penalty algorithm was started with an initial parameter of $\mu = 1$ that was iteratively increased ($\mu = 10\mu$) for each iteration until a complementarity tolerance of 10^{-6} has been achieved. For comparison, we also solved both examples with the smoothing and relaxation algorithms which, similarly, used an initial parameter of $\mu = 1$, an iterative parameterized reduction of $\mu = \mu/10$ and a complementarity tolerance of 10^{-6}. The CPU times reported are for a 3-GHz Pentium personal computer with 4 GB RAM, running WinXP.

The 4-node bilinear mixed FE of Capsoni and Corradi (1997a,b) was used to model both examples. This special element, developed using mixed variational principles, has been constructed such that various (four kinematic and two static) fields are modeled independently. The element satisfies both ellipticity and inf-sup conditions (Bathe, 2001) without any adjustable factor, and hence ensures stability and optimality of the developed discretization scheme. Some of its prominent features are: locking free behavior, stress redistribution capability during plastic spreading, weak distortion sensitivity and coarse mesh accuracy.

Our implementation of this mixed FE follows the work of Capsoni and Corradi (1997a,b) and is briefly described, in the following, for the sake of completeness.

For each generic element i, the stress field expresses the in-plane stresses $\boldsymbol{\sigma}^{i\mathrm{T}}(\mathbf{x}) \in \Re^3 = [\sigma_x, \sigma_y, \sigma_{xy}]$ as functions of the generalized stresses $\mathbf{Q}^{i\mathrm{T}} \in \Re^5 = [\,\mathbf{Q}_0^{\mathrm{T}} \quad \mathbf{Q}_1^{\mathrm{T}}\,]$ by

$$\boldsymbol{\sigma}^i = \mathbf{s}^{\mathbf{i}}(\mathbf{x})\mathbf{Q}^{\mathbf{i}}, \tag{16}$$

where

$$\mathbf{s}^{\mathbf{i}}(\mathbf{x}) = \frac{1}{\Omega}[\,\mathbf{I}_3 \quad \mathbf{s}_1(\mathbf{x})\,] \in \Re^{3\times 5},$$

$\mathbf{x} \in \Re^2 = (\xi, \eta)$ contains standard natural coordinates ranging from -1 to 1, $\mathbf{I}_3 \in \Re^{3\times 3}$ is a 3×3 identity matrix, $\mathbf{s}_1(\mathbf{x}) \in \Re^{3\times 2}$ a stress matrix, and Ω an element area. $\mathbf{Q}_0 \in \Re^3$ and $\mathbf{Q}_1 \in \Re^2$ define, respectively, constant and higher-order stress modes such that the generalized stresses $\mathbf{Q}^{\mathbf{i}}$ preclude overall rigid body motions.

Similarly, the generalized total strains $\mathbf{q}^{\mathbf{i}} \in \Re^5$ (and the generalized plastic strains $\mathbf{p}^{\mathbf{i}} \in \Re^5$) conjugate with $\mathbf{Q}^{\mathbf{i}}$ consist of constant $\mathbf{q}_0 \in \Re^3$ (and $\mathbf{p}_0 \in \Re^3$) and higher-order $\mathbf{q}_1 \in \Re^2$ (and $\mathbf{p}_1 \in \Re^2$) strain modes. Locking is ruled out by appropriately selecting the plastic strain field so that the incompressibility condition is enforced for the constant plastic strain modes. Thus, the particular in-plane plastic strains $\boldsymbol{\pi}^{i\mathrm{T}}(\mathbf{x}) \in \Re^3 = [\pi_x, \pi_y, \pi_{xy}]$ can be written as functions of $\mathbf{p}^{\mathbf{i}}$:

$$\boldsymbol{\pi}^i(\mathbf{x}) = \mathbf{h}_3^i(\mathbf{x})\mathbf{p}^{\mathbf{i}}, \tag{17}$$

where

$$\mathbf{h}_3^i(\mathbf{x}) = [\,\mathbf{I}_3 \quad \mathbf{h}_1(\mathbf{x}) + \mathbf{h}_2(\mathbf{x})\mathbf{R}\,] \in \Re^{3\times 5}.$$

$\mathbf{h}_1(\mathbf{x}) \in \Re^{3\times 2}$ defines a strain matrix, $\mathbf{h}_2(\mathbf{x}) \in \Re^{3\times 2}$ an enhanced strain matrix, and $\mathbf{R} \in \Re^{2\times 2}$ a linear transformation matrix. Descriptions of key quantities, such as $\mathbf{s}_1(\mathbf{x})$, $\mathbf{h}_1(\mathbf{x})$, $\mathbf{h}_2(\mathbf{x})$ and $\mathbf{R}$, together with elemental compatibility $\mathbf{C}^{\mathbf{i}}$ and elastic stiffness $\mathbf{E}^{\mathbf{i}}$ matrices in (1)–(3) are given in Appendix A.

When plasticity is involved, the von Mises yield criterion for plane strain problems (typically describing the failure of tensile-weak materials) are enforced at 2×2 Gauss points of each element i. The governing yield functions $\mathbf{w}^{\mathbf{i}}(\mathbf{Q}^{\mathbf{i}}, \mathbf{p}^{\mathbf{i}}, \mathbf{r}^{\mathbf{i}}) \in \Re^4$ in (5) for a perfectly plastic member i are thus

$$\mathbf{w}^{\mathbf{i}} = \int_\Omega \mathbf{L}^{\mathrm{T}}(\mathbf{x})\sqrt{\tau^i(\mathbf{x})}tJd\mathbf{x} - \mathbf{r}^{\mathbf{i}} \leqslant \mathbf{0}, \tag{18}$$

where

$$\tau^i(\mathbf{x}) = \frac{1}{2}\mathbf{Q}^{i\mathrm{T}}(\mathbf{s}^{i\mathrm{T}}(\mathbf{x})\mathbf{M}_1\mathbf{s}^{\mathbf{i}}(\mathbf{x}))\mathbf{Q}^{\mathbf{i}} - \mathbf{Q}^{i\mathrm{T}}\left(\mathbf{s}^{i\mathrm{T}}(\mathbf{x})\mathbf{M}_2\mathbf{h}_3^i(\mathbf{x})\right)\mathbf{p}^{\mathbf{i}} + \mathbf{p}^{i\mathrm{T}}\left(\mathbf{h}_3^{i\mathrm{T}}(\mathbf{x})\mathbf{M}_3\mathbf{h}_3^i(\mathbf{x})\right)\mathbf{p}^{\mathbf{i}}, \quad \mathbf{r}^{\mathbf{i}} = \int_\Omega \mathbf{L}^{\mathrm{T}}(\mathbf{x})\sigma_0 tJd\mathbf{x},$$

$$\mathbf{M}_1 = \mathbf{A}^{\mathrm{T}}\mathbf{m}\mathbf{A}, \quad \mathbf{M}_2 = E\boldsymbol{\mu}\boldsymbol{\mu}^{\mathrm{T}}, \quad \mathbf{M}_3 = \frac{E^2}{(1-2\nu)^2}\boldsymbol{\mu}\boldsymbol{\mu}^{\mathrm{T}},$$

$$\mathbf{m} = \begin{bmatrix} 2 & -1 & 0 \\ -1 & 2 & 0 \\ 0 & 0 & 6 \end{bmatrix}, \quad \mathbf{A} = \begin{bmatrix} 1-\nu & -\nu & 0 \\ -\nu & 1-\nu & 0 \\ 0 & 0 & 1 \end{bmatrix}, \quad \boldsymbol{\mu} = \begin{bmatrix} 1 \\ 1 \\ 0 \end{bmatrix}.$$

J is a determinant of the Jacobian matrix and t an elemental thickness (assumed to be of unit value).

A row matrix $\mathbf{L}(\mathbf{x}) = [\,L_1(\mathbf{x}) \quad L_2(\mathbf{x}) \quad L_3(\mathbf{x}) \quad L_4(\mathbf{x})\,]$ collects $L_g(\mathbf{x}) = 0.25(1 + 3\xi_g\xi)(1 + 3\eta_g\eta)$ for all $g \in \{1, \ldots, 4\}$, where ξ_g, η_g are the Gauss point coordinates $(\pm 1/\sqrt{3})$. The equivalent in-plane functions $\mathbf{w}^i$ in (18) describe the influences of transverse yield components through a fictitious kinematic hardening. This decreases the computational burden caused by the presence of non-vanishing transverse plastic strains π_z (Capsoni and Corradi, 1995).

The normality condition in (4) for element i can be written by

$$\frac{\partial \mathbf{w}^{i\mathrm{T}}}{\partial \mathbf{Q}^{\mathbf{i}}} = \int_\Omega \frac{(\mathbf{s}^{i\mathrm{T}}(\mathbf{x})\mathbf{M}_1\mathbf{s}^{\mathbf{i}}(\mathbf{x}))\mathbf{Q}^{\mathbf{i}} - \left(\mathbf{s}^{i\mathrm{T}}(\mathbf{x})\mathbf{M}_2\mathbf{h}_3^i(\mathbf{x})\right)\mathbf{p}^{\mathbf{i}}}{2\sqrt{\tau^i(\mathbf{x})}}\mathbf{L}(\mathbf{x})tJd\mathbf{x}. \tag{19}$$

4.1. Example 1: two blocks in frictional contact

This example consists of two plane strain rectangular blocks I and II (see Fig. 2a), supported by a smooth vertical wall and horizontal ground (Dong, 1999); v defines the horizontal displacement at the right edge of the top surface of block II.

A constant uniformly distributed force of 19.62 kN mm^{-1}) was vertically applied at upper surface GF of block I, whilst at surface

BC of block II a horizontal uniform load of 9.81α kN mm^{-1} was proportionally prescribed.

At the interface DE connecting blocks I and II, unilateral nonassociative ($\phi \neq \varphi$) Coulomb ($\varphi = 0$) frictional surfaces were adopted as in Fig. 3, where ϕ and φ denote the friction and dilatancy angles, respectively. Thus, for a contact interface k, the governing three relations (6)–(8) become

$$\mathbf{N}_n^{\mathbf{k}} = \begin{bmatrix} -\sin\phi \\ -\sin\phi \end{bmatrix}, \quad \mathbf{N}_t^{\mathbf{k}} = \begin{bmatrix} \cos\phi \\ -\cos\phi \end{bmatrix}, \quad \mathbf{V}_n^{\mathbf{k}} = \begin{bmatrix} 0 \\ 0 \end{bmatrix}, \quad \mathbf{V}_t^{\mathbf{k}} = \begin{bmatrix} 1 \\ -1 \end{bmatrix}, \quad \mathbf{r}_c^{\mathbf{k}} = \begin{bmatrix} 0 \\ 0 \end{bmatrix}. \tag{20}$$

For the elastic range, an isotropic elastic material with an elastic modulus of $E = 206$ kN mm^{-2} and a Poisson ratio of $\nu = 0.3$ was assumed.

Two sets of analysis cases, each with three friction coefficients (namely $\tan\phi = 0.25,\ 0.5$ and 1) were carried out as follows: (a) elastic only, and (b) elastic-perfectly plastic von Mises material with a yield stress of $\sigma_0 = 25$ kN mm^{-2}.

Our FE model (Fig. 2b) consists of 94 elements, 235 degrees of freedom, 470 natural generalized stresses (or strains), 376 plastic yield functions, 9 contact points and 18 contact conditions.

(a) Purely elastic. The results of stepwise holonomic analyses with an incremental step of 0.1 are displayed in Fig. 4 as $\alpha - v$ responses. The computed results agree well with the reported ones (Dong, 1999). As is clear, the initial responses are linear (elastic) and subsequently deviate from linearity as the translations are progressively activated at the contact points along DE, until the maximum load capacities were reached at $\alpha = 0.667,\ 1.333$ and 2.667 for $\tan\phi = 0.25, 0.5$ and 1, respectively.

For an imposed displacement constraint of $v \leqslant 25$ mm, we then carried out a direct limit load analysis, based on our MPEC formulation (12), for each of the three frictional coefficients. The three MPEC algorithms computed identical limit load results of

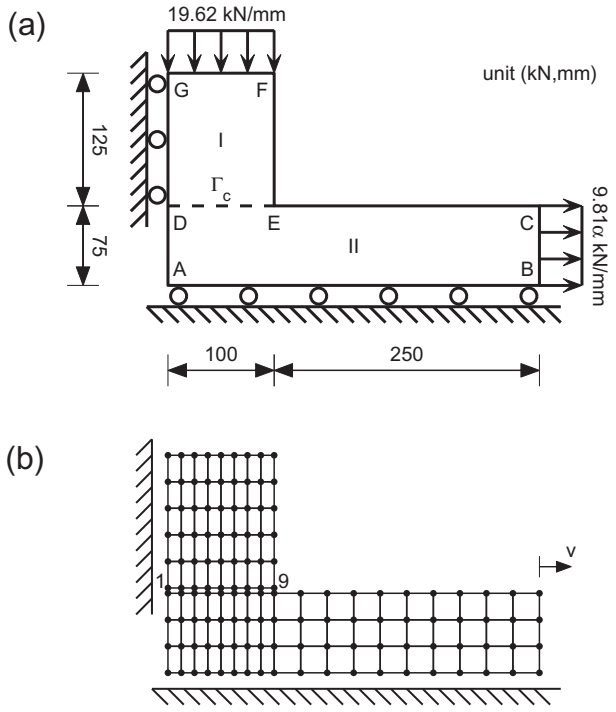

Fig. 2. Example 1: two blocks in frictional contact (a) geometry and loading, (b) mixed FE model.

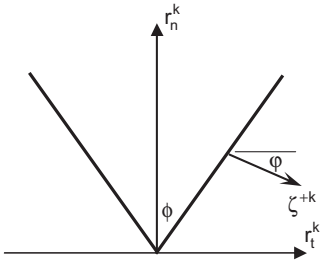

Fig. 3. Example 1: general friction law at generic frictional contact k.

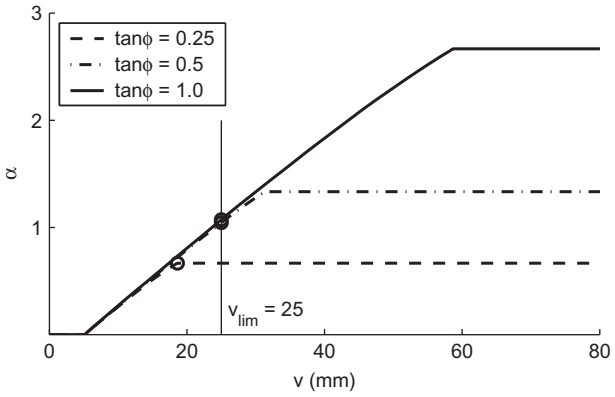

Fig. 4. Example 1: stepwise holonomic $\alpha - v$ responses of elastic blocks.

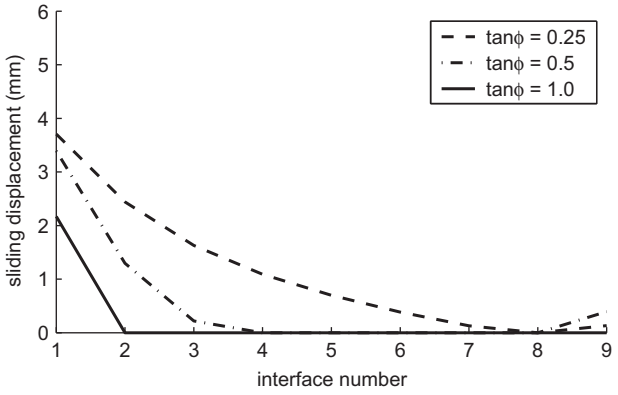

Fig. 5. Example 1: distribution of sliding interface translations at limit load of elastic blocks.

$\alpha_{\text{lim}} = 0.667,\ 1.044$ and 1.073 for $\tan\phi = 0.25,\ 0.5$ and 1, respectively. The computing times for each of the three frictional values were only a few seconds, namely 1 s, 3 s and 2 s for the penalty, smoothing and relaxation algorithms, respectively. Their accuracy is clearly validated by the associated stepwise holonomic responses, as shown in Fig. 4 (MPEC results are plotted as open dots). It should be noted that for the two higher friction values of $\tan\phi = 0.5$ and 1.0, the inclusion of this displacement constraint degrades the maximum load capacity of the structure concerned, whilst this does not influence the limit load for the low friction ($\tan\phi = 0.25$) case as the maximum load was reached before the establishment of the imposed displacement limit. Sliding interface translations associated with the limit load for each frictional case are shown in Fig. 5.

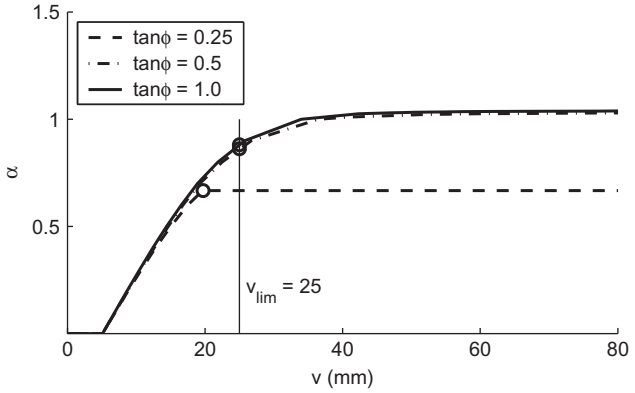

Fig. 6. Example 1: stepwise holonomic $\alpha - v$ responses of elastoplastic blocks.

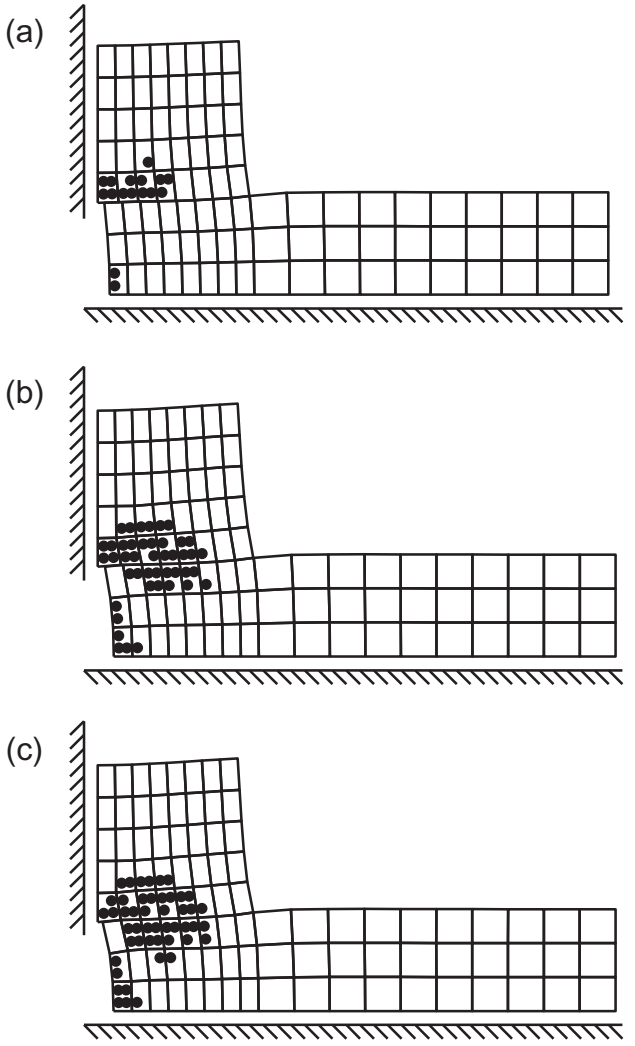

Fig. 7. Example 1: plastic locations at limit load of elastoplastic blocks (a) $\tan\phi = 0.25$, (b) $\tan\phi = 0.5$ and (c) $\tan\phi = 1.0$, where • denotes plastic zone.

(b) Elastoplastic. The results of the stepwise holonomic analyses with a finite step of 0.1 are plotted in Fig. 6, again as $\alpha - v$ curves. The influence of material nonlinearity is apparent for the higher friction values of $\tan\phi = 0.5$ and 1.0. For these instances, plastic failure occurred before failure by sliding at the interface, at the limit loads of $\alpha = 1.028$ and 1.038 for $\tan\phi = 0.5$ and 1.0, respectively. For $\tan\phi = 0.25$, on the other hand, collapse is still governed

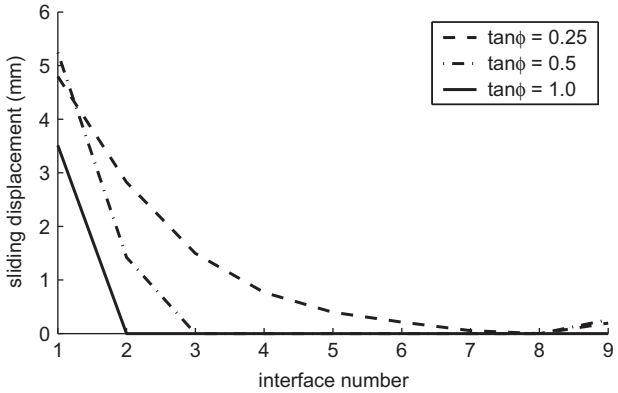

Fig. 8. Example 1: distribution of sliding contact translations at limit load of elastoplastic blocks.

(as in the purely elastic case) by sliding so that the limit load remained at $\alpha = 0.667$.

For the displacement constraint of $v \leqslant 25$ mm, each of the three proposed single-step MPEC approaches successfully computed the maximum loads of $\alpha_{\text{lim}} = 0.667,\ 0.862$ and 0.881 corresponding, respectively, to the friction coefficients of $\tan\phi = 0.25,\ 0.5$ and 1.0. The computing times reported were: 8 s (penalty), 66 s (smoothing) and 17 s (relaxation) for $\tan\phi = 0.25$; 5 s (penalty), 63 s (smoothing) and 16 s (relaxation) for $\tan\phi = 0.5$; and 4 s (penalty), 83 s (smoothing) and 15 s (relaxation) for $\tan\phi = 1$. Clearly, for this example, the penalty approach is the most efficient and robust MPEC solution scheme. The obtained results are plotted as open dots on their associated stepwise holonomic curves in Fig. 6. Locations at which plasticity developed as well as sliding contact translations corresponding to the limit load for each of the frictional cases are drawn in Figs. 7 and 8, respectively.

4.2. Example 2: concrete gravity dam

The second example concerns the safety assessment of the concrete gravity dam (ICOLD, 1999) shown in Fig. 9a, where v denotes an opening displacement at the left end of the foundation interface and h a top sway displacement at the left corner of the structure. The concrete dam is supported by a rigid rock foundation, for which both bulk concrete and foundation rock are impervious. Its structural safety is assessed as the maximum (overflow) overtopping water level, defined by α (unit-m), that can be sustained by the dam structure whilst simultaneously satisfying imposed serviceability constraints of $v \leqslant 0.06$ m and $h \leqslant 0.08$ m. At the interface Γ_c between the concrete dam and the solid foundation (see Fig. 9a), cohesive fracture can be caused by hydraulic pressure (water weight of $\gamma_w = 10$ kN m^{-3}) and is resisted by the concrete self-weight of $\gamma_c = 24$ kN m^{-3} and the interface strength. An isotropic elastic material with $E = 24 \times 10^6$ kN m^{-2} and $\nu = 0.15$ was assumed. This homogeneous plane strain structure was modeled with the bilinear mixed FE described.

In view of the isotropic elastic material assumption, the two plasticity relations (4) and (5) are eliminated, and thus the governing direct limit load formulation (13) takes the following reduced form:

$$\begin{aligned} &\text{maximize } \alpha \\ &\text{subject to } \mathbf{C}^{\mathrm{T}}\mathbf{Q} + \mathbf{C}_n^{\mathrm{T}}\mathbf{r}_n + \mathbf{C}_t^{\mathrm{T}}\mathbf{r}_t - \alpha\mathbf{f} - \mathbf{f}_d = \mathbf{0}, \\ &\qquad \mathbf{Q} - \mathbf{E}\mathbf{C}\mathbf{u} = \mathbf{0}, \\ &\qquad -\mathbf{C}_t\mathbf{u} + \mathbf{V}_t\boldsymbol{\zeta} = \mathbf{0}, \\ &\qquad -\mathbf{C}_n\mathbf{u} + \mathbf{V}_n\boldsymbol{\zeta} = \mathbf{0}, \\ &\qquad \boldsymbol{\pi}_c = -\mathbf{N}_n^{\mathrm{T}}\mathbf{r}_n - \mathbf{N}_t^{\mathrm{T}}\mathbf{r}_t + \mathbf{r}_c \geqslant \mathbf{0}, \quad \boldsymbol{\zeta} \geqslant \mathbf{0}, \quad \boldsymbol{\pi}_c^{\mathrm{T}}\boldsymbol{\zeta} = 0, \\ &\qquad \text{displacement conditions.} \end{aligned} \tag{21}$$

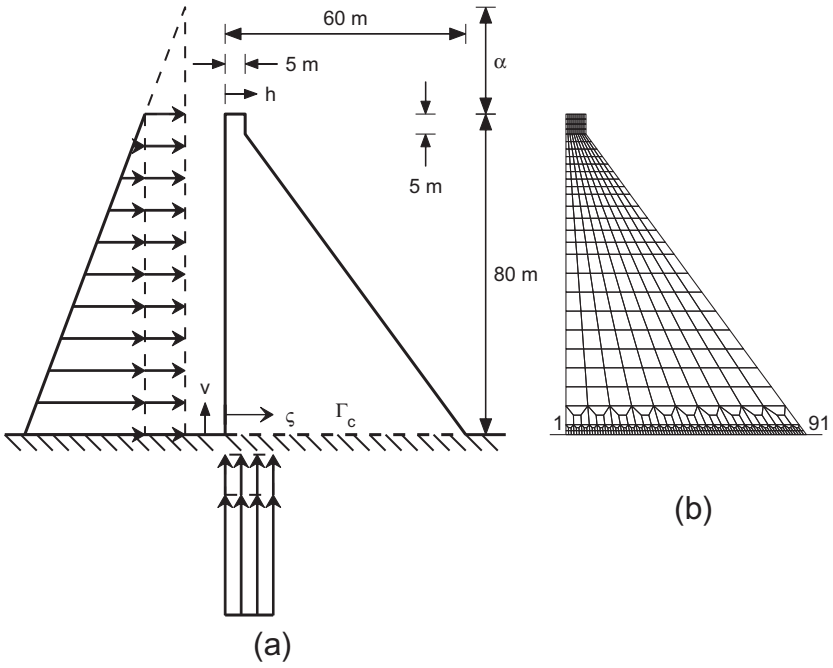

Fig. 9. Example 2: concrete gravity dam (a) geometry and loading, (b) mixed FE model.

The complementarity conditions in (21) describe crack propagation along the potential interface Γ_c.

We assumed that any fracture at interface Γ_c follows a cohesive Mode I model. For a generic interface point k, the adopted quasi-brittle fracture law is

$$\pi_c^k = r_n^k + r_c^k \geqslant 0, \quad \zeta^k \geqslant 0, \quad \pi_c^k \zeta^k = 0, \quad \text{for all } k \in \Gamma_c, \tag{22}$$

where the traction force r_n^k in (22), it is recalled, is positive in compression, the tensile traction capacity $r_c^k(\zeta^k)$ is written in terms of an auxiliary variable ζ^k and can be expressed by the following exponential traction decay:

$$r_c^k = r_o e^{-\beta \zeta^k}, \tag{23}$$

where r_o and β denote the initial tensile strength and its degrading rate, respectively. Clearly, as the damage ($\zeta^k > 0$) progresses gradually, the strength r_c^k at an interface k decays dramatically. As is often the case of an imperfect drainage system, hydraulic uplift pressure must be further considered (see Fig. 9a) at the foundation base, when a cohesive crack opening has been established ($\zeta^k > 0$). This uplift pressure $p_c^k(\zeta^k)$ is represented by an equivalent external force appropriately applied at the relevant interface point k, and takes the following form:

$$p_c^k = p_o(1 - e^{-\rho \zeta^k}), \tag{24}$$

where p_o is the water pressure at the foundation level and ρ indicates uplift pressure distribution. Obviously, $\rho = 0$ defines no uplift pressure, whilst $\rho \to \infty$ a uniform pressure distribution.

Two uplift pressure distributions, namely a perfect drainage ($\rho = 0$) and an intermediate value of $\rho = 33.33$, were studied. The prescribed cohesive fracture relations in (22)–(24) were applied to all interface points of Γ_c, where the parameters $r_o = 300$ kN-m $^{-2}$ and $\beta = 3333$ were adopted throughout.

The FE model (Fig. 9b) consists of 500 elements, 1158 degrees of freedom, 2500 generalized stresses (or strains), 91 contact points and 91 contact conditions.

Two analyses, namely a stepwise holonomic analysis with an incremental overflow step of 2 m and the proposed direct MPEC limit load approach under displacement constraints of $v \leqslant 0.06$ m and $h \leqslant 0.08$ m, were carried out. In the presence of softening, physically instabilizing and difficult to capture phenomena such as bifurcation, snapback and snapthrough behaviors can occur. We have therefore incorporated a special enumerative scheme (Tin-Loi and Tseng, 2003) to detect and capture such events (if they exist) in our stepwise holonomic algorithm.

For a perfect drainage ($\rho = 0$), the computed stepwise holonomic $\alpha - v$ (and $\alpha - h$) responses are shown as dashed lines in Figs. 10 and 11. The diagrams indicate an initial steep increase in the overall load capacity, followed later by a gradual flattening as $\alpha = 47.306$ was approached. The analysis was terminated at an excessive displacement of $v = 0.15$ m and $\alpha = 44.377$, when the overflow hydraulic pressure at the upstream face extensively promoted crack openings along the interface Γ_c.

The direct, single-step analysis was successfully solved as an MPEC. The three MPEC algorithms gave identical limit load results of $\alpha_{\text{lim}} = 37.767$, but at different computational expenses, namely 16 s, 117 s and 45 s for the penalty, smoothing and relaxation approaches, respectively. The computed result is plotted as an open dot on the associated stepwise holonomic responses in Figs. 10 and 11. The limit overflow water level obtained clearly satisfies

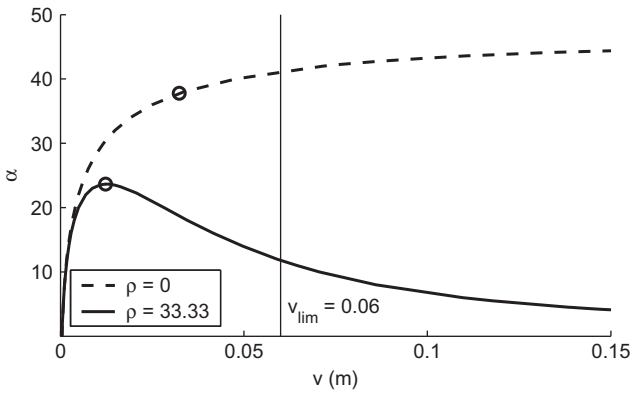

Fig. 10. Example 2: stepwise holonomic $\alpha - v$ responses.

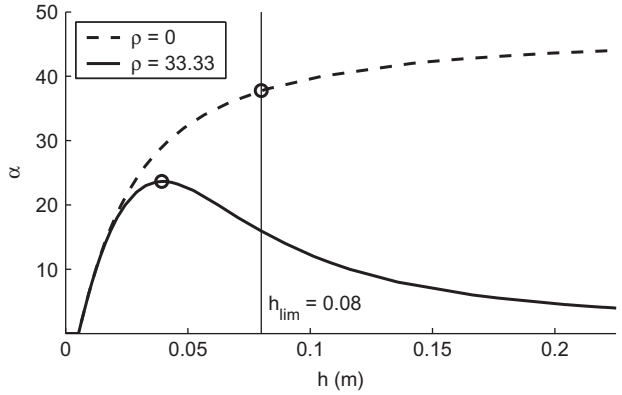

Fig. 11. Example 2: stepwise holonomic $\alpha - h$ responses.

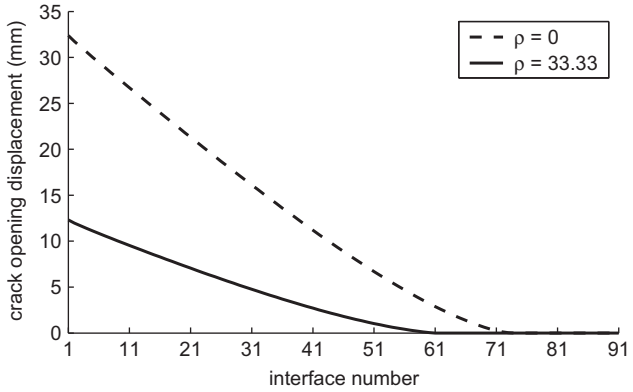

Fig. 12. Example 2: distribution of crack opening displacements at limit overflow level along Γ_c.

the displacement limits (thin lines). The corresponding crack opening distribution (dashed line) along the interface Γ_c is shown in Fig. 12.

For the imperfect drainage case, namely $\rho = 33.33$, the computed stepwise holonomic $\alpha - v$ and $\alpha - h$ curves (solid lines in Figs. 10 and 11, respectively) initially showed similar responses to those of the perfect drainage case (dashed lines). Differences later occur due to the nonlinear softening behavior assumed. The hydraulic uplift pressure acting in the crack opening induced significant reduction in the overall load capacity of the dam. A maximum overtopping water level of $\alpha = 23.643$ (with $v = 0.012$ m and $h = 0.039$ m) was attained, some 87% less when compared with the perfect drainage result. This, incidentally, emphasizes the need to incorporate hydraulic uplift pressure for a realistic safety assessment of the gravity dam to be achieved.

All three MPEC approaches for the imposed displacement conditions similarly gave $\alpha_{\text{lim}} = 23.643$. Once again, the penalty algorithm consumed significantly less computing resources, namely only 20 s, as compared to the smoothing (110 s) and relaxation (43 s) approaches. The result is shown as an open dot on the associated stepwise holonomic curves in Figs. 10 and 11. For this case, the imposed serviceability requirements did not affect the maximum overtopping water capacity of the structure concerned, since the peak water level was actually reached prior to the attainment of limited displacements. The crack opening displacement distribution along interface Γ_c corresponding to this limit is shown as a solid line in Fig. 12.

5. Concluding remarks

This paper presents a direct optimization approach to evaluate the maximum load of structures that are subjected to simultaneous contact and displacement limitation conditions. The proposed scheme preserves the distinctive and appealing feature of classical limit analysis in that it furnishes efficiently and robustly, in a single step analysis, an upper bound to the maximum load of the structure. Two contact-like mechanics applications, namely unilateral Coulomb frictional contact of multi elastoplastic bodies and a cohesive fracture along potential failure interfaces, have been the focus of this study. Such problems are difficult to handle by marching (step-by-step) analyses: the former involves nonassociative Coulomb friction (no dilation during sliding), whilst the latter involves the instabilizing, softening effects caused by the decay of tractions within the process zone.

The governing formulation for our extended limit analysis approach takes the form of a challenging class of mathematical programs, known as an MPEC. It is well-known that the presence of complementarity constraints (in our case arising from the plastic constitution and contact requirements) can pose formidable computational challenges for its solution. However, drawing on our previous computational experience in the solution of MPECs in engineering mechanics, we successfully processed the MPEC, transformed into a standard, but iterative, NLP problem using a suitable parametric reformulation. Of these transformation schemes, the penalty NLP-based algorithm appears to be the most robust and effective and successfully solved all problem instances we have tried.

Two examples, often used in the contact and fracture literature, are given to illustrate application of the MPEC approach. All FE models have been constructed using our implementation of a plane strain mixed FE, the key ideas of which were developed by Capsoni and Corradi (1997a,b). Such an element offers various benefits, the main ones being a locking free capability and coarse mesh accuracy. The MPEC results have been validated for their accuracy through a comparison with the corresponding stepwise holonomic responses.

Straightforward yet fruitful extension of the present work includes application of the MPEC approach to other important engineering mechanics problems, such as mixed mode fracture; 3D FE problems; and elastoplastic plates and shells often used as energy absorbers or bumpers and for which the effects, on maximum load capacity, of potentially large deformations or energy dissipation may need to be assessed.

Acknowledgement

This research was supported by the Australian Research Council through ARC Discovery Grant DP0986332.

Appendix A. Descriptions of key quantities for mixed FE (Capsoni and Corradi, 1997a,b)

For an isoparametric 4-node bilinear element i, the actual and natural coordinates are defined as $\mathbf{X} \in \Re^2 = (X, Y)$ and $\mathbf{x} \in \Re^2 = (\xi, \eta)$, respectively. Both the nodal and natural coordinates for each element i are collected in the vector forms:

$$\mathbf{X}_i = \begin{bmatrix} X_1 \\ X_2 \\ X_3 \\ X_4 \end{bmatrix}, \quad \mathbf{Y}_i = \begin{bmatrix} Y_1 \\ Y_2 \\ Y_3 \\ Y_4 \end{bmatrix}, \quad \boldsymbol{\xi}_i = \begin{bmatrix} -1 \\ 1 \\ 1 \\ -1 \end{bmatrix}, \quad \boldsymbol{\eta}_i = \begin{bmatrix} -1 \\ -1 \\ 1 \\ 1 \end{bmatrix}. \tag{A.1}$$

The Jacobian matrix $\mathbf{J}(\mathbf{x}) \in \Re^{2\times 2}$ is

$$\mathbf{J}=\begin{bmatrix} J_{11} & J_{12} \\ J_{21} & J_{22} \end{bmatrix}, \tag{A.2}$$

where $J_{11}=0.25\mathbf{X}_i^{\mathrm{T}}(\xi_i+\eta\mathbf{c})$, $J_{12}=0.25\mathbf{Y}_i^{\mathrm{T}}(\xi_i+\eta\mathbf{c})$, $J_{21}=0.25\mathbf{X}_i^{\mathrm{T}}(\boldsymbol{\eta}_i+\xi\mathbf{c})$, $J_{22}=0.25\mathbf{Y}_i^{\mathrm{T}}(\boldsymbol{\eta}_i+\xi\mathbf{c})$ and $\mathbf{c}^{\mathrm{T}}=[1\quad -1\quad 1\quad -1]$. Then, the determinant $J(\mathbf{x})$ of the Jacobian matrix can be written as

$$J=J^0+\xi J_\xi+\eta J_\eta, \tag{A.3}$$

where $J^0=\mathbf{Y}_i^{\mathrm{T}}\mathbf{m}^0\mathbf{X}_i$, $J_\xi=\mathbf{Y}_i^{\mathrm{T}}\mathbf{m}_\xi\mathbf{X}_i$, $J_\eta=\mathbf{Y}_i^{\mathrm{T}}\mathbf{m}_\eta\mathbf{X}_i$, $\mathbf{m}^0\in\Re^{4\times4}=(\boldsymbol{\eta}_i\boldsymbol{\xi}_i^{\mathrm{T}}-\boldsymbol{\xi}_i\boldsymbol{\eta}_i^{\mathrm{T}})/16$, $\mathbf{m}_\xi\in\Re^{4\times4}=(\mathbf{c}\boldsymbol{\xi}_i^{\mathrm{T}}-\xi_i\mathbf{c}^{\mathrm{T}})/16$ and $\mathbf{m}_\eta\in\Re^{4\times4}=(\boldsymbol{\eta}_i\mathbf{c}^{\mathrm{T}}-\mathbf{c}\boldsymbol{\eta}_i^{\mathrm{T}})/16$. We further define the transformation matrix $\mathbf{T}(\mathbf{x})\in\Re^{3\times3}$ as

$$\mathbf{T}=\begin{bmatrix} J_{11}^2 & J_{21}^2 & 2J_{11}J_{21} \\ J_{12}^2 & J_{22}^2 & 2J_{12}J_{22} \\ J_{11}J_{12} & J_{21}J_{22} & J_{11}J_{22}+J_{12}J_{21} \end{bmatrix}. \tag{A.4}$$

It is noted that a superscript 0 denotes the values of the relevant quantities calculated at the element centroid, e.g. $J^0=J(0,0)$ and $\mathbf{T}^0=\mathbf{T}(0,0)$.

Therefore, the key matrices $\mathbf{s}_1(\mathbf{x})$, $\mathbf{h}_1(\mathbf{x})$ and $\mathbf{h}_2(\mathbf{x})$ in (16) and (17) are defined by

$$\mathbf{s}_1(\mathbf{x})=\mathbf{T}^0\begin{bmatrix} 3\eta-J_\eta/J^0 & 0 \\ 0 & 3\xi-J_\xi/J^0 \\ 0 & 0 \end{bmatrix}, \tag{A.5}$$

$$\mathbf{h}_1(\mathbf{x})=\frac{J^0}{J}(\mathbf{T}^0)^{-\mathrm{T}}\begin{bmatrix} \eta & 0 \\ 0 & \xi \\ 0 & 0 \end{bmatrix}, \tag{A.6}$$

$$\mathbf{h}_2(\mathbf{x})=\frac{J^0}{J}(\mathbf{T}^0)^{-\mathrm{T}}\begin{bmatrix} \xi & 0 \\ 0 & \eta \\ 0 & 0 \end{bmatrix}. \tag{A.7}$$

The description of $\mathbf{R}$ in (17) satisfies the following relationship:

$$\boldsymbol{\mu}^{\mathrm{T}}(\mathbf{h}_1(\mathbf{x})+\mathbf{h}_2(\mathbf{x})\mathbf{R})=\mathbf{0}, \tag{A.8}$$

where $\boldsymbol{\mu}^{\mathrm{T}}=[1\quad 1\quad 0]$.

The element compatibility matrix $\mathbf{C}^{\mathbf{i}}\in\Re^{5\times8}$ in (1) and (2) is

$$\mathbf{C}^{\mathbf{i}}=\begin{bmatrix} \boldsymbol{\beta}_\xi & \mathbf{0} & \boldsymbol{\beta}_\eta & J_{11}^0\gamma & J_{21}^0\gamma \\ \mathbf{0} & \boldsymbol{\beta}_\eta & \boldsymbol{\beta}_\xi & J_{12}^0\gamma & J_{22}^0\gamma \end{bmatrix}^{\mathrm{T}}, \tag{A.9}$$

where the vectors $\boldsymbol{\alpha},\boldsymbol{\beta}_\xi,\boldsymbol{\beta}_\eta,\gamma\in\Re^{1\times4}$ are obtained by

$$\begin{bmatrix}\boldsymbol{\alpha} & \boldsymbol{\beta}_\xi & \boldsymbol{\beta}_\eta & \gamma\end{bmatrix}^{\mathrm{T}}=\begin{bmatrix}\mathbf{a} & \mathbf{X}_i & \mathbf{Y}_i & \mathbf{c}\end{bmatrix}^{-1} \tag{A.10}$$

and $\mathbf{a}^{\mathrm{T}}=[1\quad 1\quad 1\quad 1]$. Finally, the element stiffness matrix $\mathbf{E}^{\mathbf{i}}\in\Re^{5\times5}$ in (3) is given as follows:

$$\mathbf{E}^{\mathbf{i}}=\begin{bmatrix} \Omega t\mathbf{D} & \mathbf{0} \\ \mathbf{0} & \mathbf{E}_{11}-\mathbf{E}_{12}\mathbf{E}_{22}^{-1}\mathbf{E}_{21} \end{bmatrix}, \tag{A.11}$$

where $\mathbf{E}_{ab}\in\Re^{2\times2}=\int_\Omega\mathbf{h}_a^{\mathrm{T}}(\mathbf{x})\mathbf{D}\mathbf{h}_b(\mathbf{x})tJd\mathbf{x}$ and $\mathbf{D}\in\Re^{3\times3}$ is the classical element elastic matrix of an isotropic (plane stress or plane strain) material. The complete expressions and derivations for this mixed FE can be found in Capsoni and Corradi (1997a,b).

References

Alfano, G., Marfia, S., Sacco, E., 2006. A cohesive damage–friction interface model accounting for water pressure on crack propagation. Computer Methods in Applied Mechanics and Engineering 196, 192–209.

Ardito, R., Cocchetti, G., Maier, G., 2008. On structural safety assessment by load factor maximization in piecewise linear plasticity. European Journal of Mechanics A/Solids 27, 859–881.

Bathe, K.J., 2001. The inf–sup condition and its evaluation for mixed finite element methods. Computers and Structures 79, 243–252.

Bellemare, S., Dao, M., Suresh, S., 2007. The frictional sliding response of elasto-plastic materials in contact with a conical indenter. International Journal of Solids and Structures 44, 1970–1989.

Bolzon, G., 2010. Collapse mechanisms at the foundation interface of geometrically similar concrete gravity dams. Engineering Structures 32, 1304–1311.

Bolzon, G., Cocchetti, G., 2003. Direct assessment of structural resistance against pressurized fracture. International Journal for Numerical and Analytical Methods in Geomechanics 27, 353–378.

Brooke, A., Kendrick, D., Meeraus, A., Raman, R., 1998. GAMS: A User's Guide. GAMS Development Corporation, Washington, DC.

Capsoni, A., Corradi, L., 1995. A plane strain formulation of the elastic-plastic constitutive law for hardening von mises materials. International Journal of Solids and Structures 32, 3515–3531.

Capsoni, A., Corradi, L., 1997a. A mixed finite element model for plane strain elastic-plastic analysis. Part I: formulation and assessment of the overall behaviour. Computer Methods in Applied Mechanics and Engineering 141, 67–79.

Capsoni, A., Corradi, L., 1997b. A mixed finite element model for plane strain elastic-plastic analysis. Part II: application to the 4-node bilinear element. Computer Methods in Applied Mechanics and Engineering 141, 81–93.

Christensen, P.W., 2002. A semi-smooth newton method for elasto-plastic contact problems. International Journal of Solids and Structures 39, 2323–2341.

Cottle, R.W., Pang, J.S., Stone, R.E., 1992. The Linear Complementarity Problem. Academic Press, San Diego, CA.

Dirkse, S.P., Ferris, M.C., 1995. PATH solver: a nonmonotone stabilization scheme for mixed complementarity problems. Optimization Methods and Software 5, 123–156.

Dirkse, S.P., Ferris, M.C., 1995. MCPLIB: a collection of nonlinear mixed complementarity problems. Optimization Methods and Software 5, 319–345.

Dong, C.Y., 1999. A simple benchmark problem to test frictional contact. Computer Methods in Applied Mechanics and Engineering 177, 153–162.

Drud, A.S., 1994. CONOPT-a large-scale GRG code. ORSA Journal on Computing 6, 207–216.

Ferris, M.C., 1998. MATLAB and GAMS: interfacing optimization and visualization software, Technical Report TR98-19. Computer Sciences Department, University of Wisconsin, Madison, Wisconsin.

Ferris, M.C., Pang, J.S., 1997. Engineering and economic applications of complementarity problems. SIAM Review 39, 669–713.

Ferris, M.C., Tin-Loi, F., 2001. Limit analysis of frictional block assemblies as a mathematical program with complementarity constraints. International Journal of Mechanical Sciences 43, 209–224.

Giambanco, G., Rizzo, S., Spallino, R., 2001. Numerical analysis of masonry structures via interface models. Computer Methods in Applied Mechanics and Engineering 190, 6493–6511.

Gilbert, M., Casapulla, C., Ahmed, H.M., 2006. Limit analysis of masonry block structures with non-associative frictional joints using linear programming. Computers and Structures 84, 873–887.

ICOLD, 1999. Theme A2, Imminent failure flood for a concrete gravity dam. In: 5th International Benchmark Workshop on Numerical Analysis of Dams, Denver.

Kamenjarzh, J.A., 1996. Limit Analysis of Solids and Structures. CRC Press, Boca Raton.

Kanno, Y., Ohsaki, M., 2011. A non-interior implicit smoothing approach to complementarity problems for frictionless contacts. Computer Methods in Applied Mechanics and Engineering 200, 1176–1185.

Kanzow, C., 1996. Some noninterior continuation methods for linear complementarity problems. SIAM Journal on Matrix Analysis and Applications 17, 851–868.

Luo, Z.Q., Pang, J.S., Ralph, D., 1996. Mathematical Programs with Equilibrium Constraints. Cambridge University Press, Cambridge.

Maier, G., 1970. A matrix structural theory of piecewise linear elastoplasticity with interacting yield planes. Meccanica 5, 54–66.

Maier, G., 1984. Mathematical programming applications to structural mechanics: some introductory thoughts. Engineering Structures 6, 2–6.

Maier, G., Munro, J., 1982. Mathematical programming applications to engineering plastic analysis. Applied Mechanics Reviews 35, 1631–1643.

Maier, G., Novati, G., Cen, Z., 1993. Symmetric Galerkin boundary element method for quasi-brittle-fracture and frictional contact problems. Computational Mechanics 13, 74–89.

Rutherford, T.F., 1995. Extension of GAMS for complementarity problems arising in applied economic analysis. Journal of Economic Dynamics and Control 19, 1299–1324.

Simo, J.C., Hughes, T.J.R., 1998. Computational Inelasticity. Springer-Verlag, New York.

Simo, J.C., Taylor, R.L., 1985. Consistent tangent operators for rate-independent elastoplasticity. Computer Methods in Applied Mechanics and Engineering 48, 101–118.

Tangaramvong, S., Tin-Loi, F., 2007. A complementarity approach for elastoplastic analysis of strain softening frames under combined bending and axial force. Engineering Structures 29, 742–753.

Tangaramvong, S., Tin-Loi, F., 2011a. Collapse load evaluation of structures with frictional contact supports under combined stresses. Computers and Structures 89, 1050–1058.

Tangaramvong, S., Tin-Loi, F., 2011b. Mathematical programming approaches for the safety assessment of semirigid elastoplastic frames. International Journal of Solids and Structures 48, 1011–1023.

Tangaramvong, S., Tin-Loi, F., Senjuntichai, T., 2011. An MPEC approach for the critical post-collapse behavior of rigid-plastic structures. International Journal of Solids and Structures 48, 2732–2742.

Tin-Loi, F., Que, N.S., 2001. Parameter identification of quasibrittle materials as a mathematical program with equilibrium constraints. Computer Methods in Applied Mechanics and Engineering 190, 5819–5836.

Tin-Loi, F., Tseng, P., 2003. Efficient computation of multiple solutions in quasibrittle fracture analysis. Computer Methods in Applied Mechanics and Engineering 192, 1377–1388.

Tin-Loi, F., Xia, S.H., 2001. Nonholonomic elastoplastic analysis involving unilateral frictionless contact as a mixed complementarity problem. Computer Methods in Applied Mechanics and Engineering 190, 4551–4568.